American Journal of Pathology, Vol. 146, No. 2, February 1995

Differential Permeability and Quantitative MR Imaging of a Human Lung Carcinoma Brain Xenograft in the Nude Rat

Peggy A. Barnett,* Simon Roman-Goldstein,† Fred Ramsey,‡ Christopher I. McCormick,* Gary Sexton,§ Jerzy Szumowski,† and Edward A. Neuwelt*‖

From the Departments of Neurology and Diagnostic Radiology,† the Departments of Surgery, Medicine, and Public Health,§ and the Departments of Neurosurgery and Biochemistry and Molecular Biology,‖ and the Oregon Health Sciences University, Portland, Oregon; Department of Statistics,‡ Oregon State University, Corvallis, Oregon*

This study characterized agent differential permeability, three-dimensional tumor volume, and survival in an LX-1 human small cell lung carcinoma intracerebral xenograft model in the nude rat. The percent accessible tissue space (distribution volume) and the permeability × capillary surface product for aminoisobutyric acid (M_r 103), methotrexate (M_r 454), dextran 10 (M_r 10,000), and dextran 70 (M_r 70,000) were measured between 8 and 16 days after inoculation of tumor. Magnetic resonance imaging and histology were used to quantitate intracerebral tumor volume (mm^3). Accessible tissue space (ml/g) and permeability × capillary surface product in intracranial tumor, surrounding brain, and subcutaneous tumor decreased with increasing molecular weight of the agent, regardless of the number of days after inoculation. Accessible tissue space in intracranial tumor increased between 8 and 16 days for all agents except dextran 70. There was little change in the subcutaneous tumor or other tissues with time. Tumor volume calculations from imaging studies correlated with volumetric measurements from histological sections (r^2 = 98.5%) and illustrated natural tumor progression (9 to 225 mm^3). These results provide a basis for therapeutic design based on differential permeability of specific agents and the ability to quantitatively measure brain tumor volume for accessing tumor response. (Am J Pathol 1995, 146:436–449)

There is general agreement in the field of malignant brain tumor research that therapeutic progress has been modest in part because human tumors are characterized by a variable integrity of the blood-brain barrier (BBB). Numerous animal and clinical studies with computed tomography and magnetic resonance (MR) imaging have documented variable permeability associated with different tumor types, regional variability within individual tumors, and changes in the tumor periphery.[1–6] Recently, clinical studies of quantitative measurements of the blood-to-tissue transfer constant (k_1) have verified this variable permeability.[7] In 1992, Zhang and colleagues[8] reported permeability increases related to tumor size using the small M_r marker fluorescein based on eight different human cell lines grown in a nude mouse brain metastasis model. The current communication confirms increasing permeability with tumor size and extends this observation to demonstrate permeability differences with four agents with varying characteristics, in particular a broad range of molecular weights. Differential permeability to various markers has therapeutic application in at least two potential models.[9–14]

One application depends on the differential permeability of brain tumors to drugs as compared with antibodies. That is, chemotherapeutic agents are generally low molecular weight molecules, to which brain tumors tend to be more permeable.[15] The subsequent administration of antibody that binds and inactivates the effects of chemotherapy outside of the central nervous system may allow the rescue of sys-

Supported by the Veterans Administration Merit Review Grant and the National Institutes of Health Grant R01 31770-10.

Accepted for publication October 25, 1994.

Address reprint requests to Dr. Edward A. Neuwelt, Oregon Health Sciences University, Department of Neurology, L603, 3181 SW Sam Jackson Park Road, Portland, OR 97201.

temic toxic effects.[11] Thus, drug inactivation with antibodies[12] is under investigation on the basis that brain tumors are much less permeable to higher molecular weight agents. Initial studies on the basis of this concept have been performed in a brain abscess model.[16]

Another application of differential permeability is the use of an enzyme (ie, alkaline phosphatase) bound to a tumor-specific antibody, as demonstrated by Senter and co-workers,[13,14] to form a relatively high-molecular-weight molecule. This conjugate can be delivered across the BBB with osmotic disruption.[17] The conjugate then binds to tumor surface antigens and the BBB returns to the predisrupted condition. A low molecular weight, less toxic prodrug (ie, phosphorylated) capable of being activated to the cytotoxic agent by the antibody-enzyme conjugate is then given in high doses, resulting in localized drug activation and therapy.

The measurement of tumor volumes for determining efficacy in animal models has also stimulated recent interest.[18,19] Animal studies of brain tumor therapy have previously relied primarily on survival (which is complicated by numerous covariables) and histology, both of which are limited to end-point measurements.[15,20–22] Clinical efficacy is measured by tumor response on contrast-enhanced computed tomography and MR imaging as well as survival and pathology. The ability to analyze treatment efficacy in an animal brain tumor model could be greatly expanded by the ability to perform multiple noninvasive *in vivo* imaging studies and monitor three-dimensional tumor volumes.

Based on the need for new effective agents and strategies for brain tumor therapy, the present study characterized an intracerebral human LX-1 small cell lung carcinoma (SCLC) xenograft model, a common brain metastasis. Differential permeability to agents of varying molecular weight, three-dimensional tumor volumes associated with disease progression as measured by both histology and MR imaging, and survival were measured. In addition to demonstrating tumor permeability changes, this model provides a measurement basis for therapy studies with noninvasive MR imaging to obtain tumor volume measurements.

Materials and Methods

Animal Tumor Model

Female athymic nude rats from a colony maintained at the Oregon Health Sciences University were used for all studies. LX-1 human SCLC cells were grown in culture and harvested as previously described.[23] Cell viability was >85% as determined by trypan blue exclusion. With minor modifications, LX-1 cells were stereotactically inoculated as previously described.[24] Intracerebral location was determined by precise stereotactic coordinates: 0 = Bregma; lateral = −0.31 cm (right); vertical = −0.65 cm (down from skull surface). Anatomical location was deep in the caudate putamen. In each animal, 10 µl (8×10^5 cells) and 500 µl (4×10^7 cells) of the prepared suspension were inoculated into the right hemisphere and subcutaneously into the right flank, respectively.

Differential Permeability Study

This study was designed to evaluate intracerebral tumor permeability to diverse agents with a wide range of molecular weights (greater than two logs) during natural tumor progression. The agents used were [^{14}C]aminoisobutyric acid (AIB) (M_r 103), [^{3}H]methotrexate (MTX) (M_r 454), [^{14}C]dextran 10 (DEX10) (M_r 10,000), and [^{14}C]dextran 70 (DEX70) (M_r 70,000). Five different time points after inoculation of LX-1 cells were evaluated for each agent (8, 10, 12, 14, and 16 days). Experimental groups were randomly established by agent and time. Animals were anesthetized with sodium pentobarbital (50 mg/kg, i.p.) and a catheter placed in the right femoral vein for plasma collection. Evans blue (2%, 2 ml/kg) and fluorescein (10%, 0.12 ml) were given i.v. as marker dyes of intracerebral tumor to aid in the excision of samples for scintillation counting.[24] After i.v. agent administration (10 µCi), a plasma sample was obtained immediately and at 2, 4, 6, 8, and 10 minutes. Animals were sacrificed at 10 minutes after agent administration.

By regional brain sampling, the following tissues were obtained for scintillation counting: intracerebral tumor (ICT), brain around tumor (BAT; 2- to 3-mm edge around tumor), ipsilateral brain distant to tumor (BDT), contralateral normal brain (LH; left hemisphere), and subcutaneous tumor (SQT). All samples were corrected for quench and background activity obtained from tissue controls.

Tumor Volume Study

The purpose of this study was to measure three-dimensional histological tumor volumes during untreated tumor progression and to evaluate the potential of using MR imaging to measure tumor volume. In

a random design concurrent with the differential permeability study, tumor-bearing animals were sacrificed at 8, 10, 12, 14, or 16 days after inoculation for histological tumor volume calculation. For MR imaging tumor volume analysis, animals were scanned at 8, 10, 12, 14, 15, 16, or 18 days after inoculation (n = 9); histological tumor volumes were also determined after each imaging study. A total of 25 animals were processed for histological volume.

MR imaging studies were performed on a 1.5 Tesla GE Signa unit (General Electric, Milwaukee, WI) with a compatible custom engineered loop-gap resonator coil. Serial coronal MR images (0.7 mm) were obtained through the whole brain in a volume acquisition mode with a T2-weighted gradient-recalled echo sequence (repetition time, 50; echo delay time, 12; number of excitations, 2; flip angle, 60°) with a 256 × 192 matrix and a 9-cm field of view. Gadopentetate dimeglumine (7 mmol/m^2) (Magnevist, Berlex Imaging, Wayne, NJ) was administered i.v. before imaging (corresponding to a human dose of 0.2 mmol/kg). Magnetic resonance data was acquired in digital form and transferred to a MAC IICi computer for numerical analysis.

After formalin fixation, histological sections for volume determination were obtained from 0.1-mm consecutive coronal vibratome slices through the entire intracerebral tumor. Sections were stained with hematoxylin and eosin and mounted on gelatin slides. With a Zeiss Axioplan microscope under low magnification with a Sony CCD/RGB DXC 151 camera attached, whole coronal sections were converted from analog to digital images.

MR images and digitized histological sections were analyzed with IMAGE 1.42 software (Wayne Rasband, Research Services Branch, National Institute of Mental Health, Bethesda, MD). Tumor was defined for each image or section as pixel values >3 SD from a normal contralateral brain reference. Volumes (mm^3) were calculated from calibration curves.

Survival Study

A survival study of untreated animals (n = 19) was performed for the determination of the natural progression of this tumor model. Concurrently with the permeability and volume studies, animals were periodically inoculated and followed until death. When tissue preservation after death was possible, animals were also processed for histological tumor volume (n = 7).

Data Analysis

In the permeability study, data are expressed as percent accessible tissue space (ml/g). The percent accessible tissue space is a volume distribution measure consisting of both intravascular and extravascular components (disintegrations per minute (dpm)/g tissue/dpm/ml plasma) × 100). This is similar to the tissue space measurements of Reed and Woodbury.[25] Thus, if the brain and plasma concentrations are equal, the value is 100%. Forty study animals were randomly assigned in duplicate to a 4 × 5 factorial design. The factors were agents (AIB, MTX, DEX10, and DEX70) and days postinoculation 8, 10, 12, 14, and 16. For estimating the rate of change (slope) of tissue permeability (percent accessible tissue space), an unbiased estimate, based on 10 animals, was obtained for each agent by fitting a least squares regression model with an indicator variable for each agent in the usual manner.[26,27] Percent accessible tissue space was expressed on a log scale to stabilize the variances before fitting the model. The regression model was also used to determine differences among the fitted values at 8 and 16 days after intracerebral inoculation (ie, intercepts). The reference agent in the regression model was taken to be the large intravascular marker DEX70. Details of the regression model are found in the Appendix. If there were significant differences in the slope, the 16-day intercept was also calculated. Both the raw data (point) and regression data (line) are presented. The accessible tissue space measure does not correct for the marker that is intravascular in the tissue.

Even though the intravascular plasma space is heterogeneous in central nervous system tumors, a functional expression of capillary permeability, the cerebrovascular permeability P (cm sec^1) × capillary surface area S (cm^{2}g^{-1} brain, or cm^{-1}) was also calculated at selected time points[28–30]:

$$PS = \frac{C_{\text{tissue}}(T) - V_B}{\int_0^T (C_{\text{pls}}\, dt)}$$

where C_{tissue} is the measured agent activity (dpm/g) at the time of death (T), C_{pls} is the plasma concentration (dpm/ml), and V_B is the intravascular plasma space. For calculating PS for MTX the denominator of this equation included a correction for unbound MTX in plasma (0.50).[31] V_B was calculated from DEX70 because it is a poorly penetrating solute over the 10-minute measurement period and did not change dur-

ing the experimental period of 8 to 16 days after inoculation[30]:

$$V_B = \left(\frac{C_{tissue}}{Plasma(T)}\right)_{DEX70} \times Plasma(T)_{agent}$$

where

$$\left(\frac{C_{tissue}}{Plasma(T)}\right)_{DEX70}$$

corresponds to the tissue sample for which PS is calculated and at the same day after inoculation.

Results

Permeability Study

In the permeability study, there are three major data components: 1), effect of the number of days after inoculation (tumor progression); 2), differences between the agents within a given tissue (differential permeability); and 3), the differences of a given agent within all tissues (tissue permeability).

In intracerebral tumor (ICT), the effect of the number of days after inoculation of tumor cells for each of the four agents on the percent accessible tissue space (ml/g) is shown in Figure 1A. By multiple regression analysis, the data were model fitted (r^2 = 0.9464). Compared with the large molecular weight intravascular DEX70 control, there was a significant increase (line slope) in the percent accessible tissue space for AIB (P = 0.0251) and MTX (P = 0.0394) and a marginally significant increase for DEX10 (P = 0.0513) during tumor progression between 8 and 16 days after inoculation (Table 1). During the experimental period, accessible tissue space increased 120, 108 and 93% for AIB, MTX, and DEX10, respec-

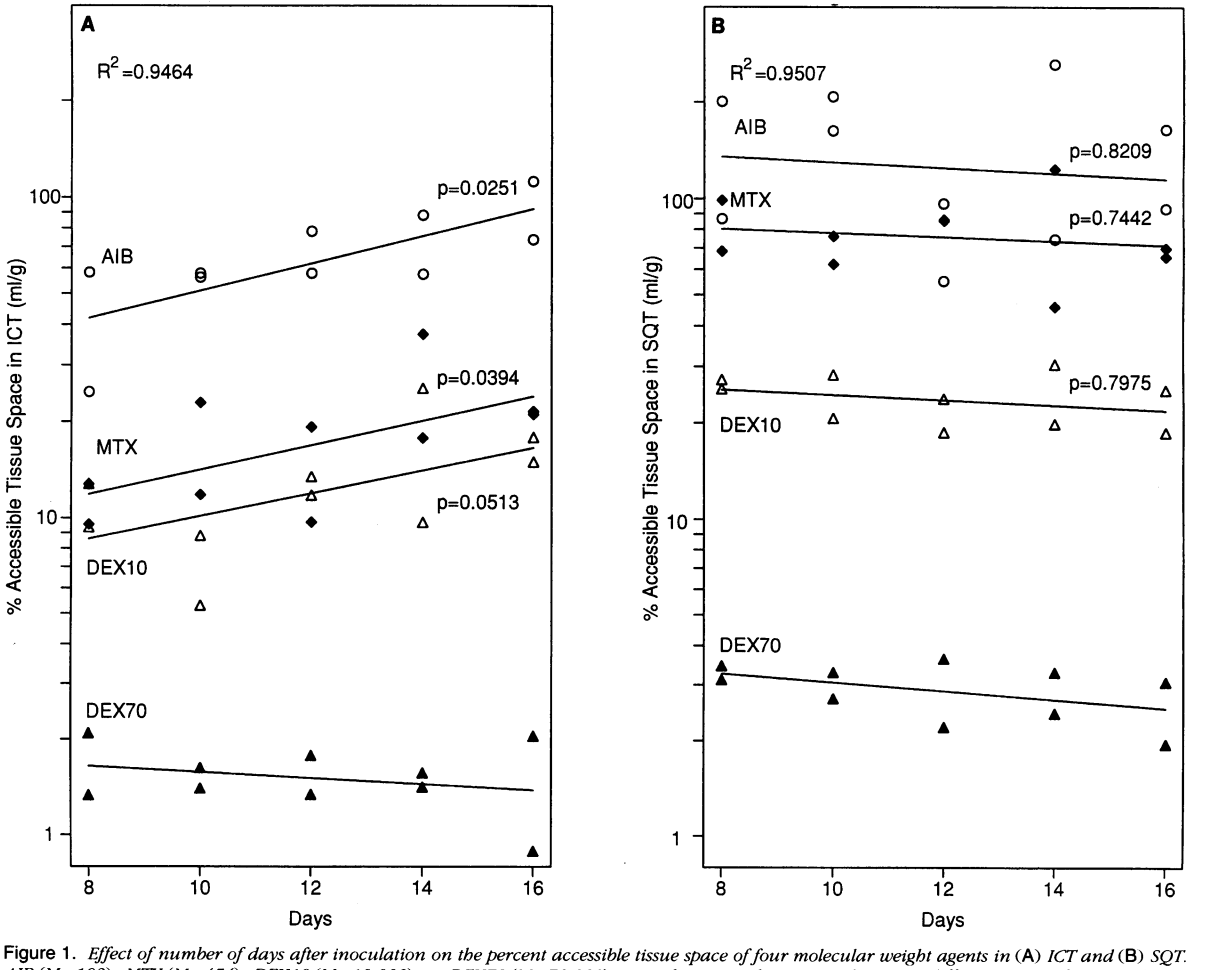

Figure 1. *Effect of number of days after inoculation on the percent accessible tissue space of four molecular weight agents in* (A) *ICT and* (B) *SQT. AIB* (M_r *103), MTX* (M_r *454), DEX10* (M_r *10,000), or DEX70* (M_r *70,000) was administered i.v. in nude rats at different times after inoculation with human LX-1 SCLC cells. Animals were sacrificed 10 minutes after agent administration.* R^2 *is the coefficient of correlation. The listed* P (p) *values compare the slope of regression lines of AIB, MTX, and DEX10 with the slope of the line for the large intravascular marker, DEX70.* ○, *AIB;* ◆, *MTX;* △, *DEX10;* ▲, *DEX70.*

Table 1. *Rates of Change (Slope) and Levels (Intercept) of Percent Accessible Tissue Space (ml/g) in Figures 1 and 2**

Tissue	Statistical parameter*	AIB	MTX	DEX10	DEX70
ICT	8-day intercept	41.88	11.85	8.60	1.65
	16-day intercept†	92.30	24.05	16.61	1.39
	Slope	1.104	1.092	1.086‡	0.979‡
BAT	8-day intercept	14.29	6.90	5.57	0.92
	Slope	1.008	0.983	1.071	1.011
BDT	8-day intercept	8.58	4.33	5.87	0.87
	Slope	1.011	1.000	1.049	1.013
LH	8-day intercept	10.30	4.30	5.67	0.76
	Slope	0.999	1.001	1.056	1.038
SQT	8-day intercept	135.30§	80.30§	25.36	3.26
	Slope	0.980	0.986	0.982	0.969

*Multiple regression analysis was used to determine differences in the rate of change (slope) among agents and the differences between agents (8-day *y* intercept as determined by the regression line, n = 10) within a given tissue. When there were significant differences in slope, the 16-day intercept was also calculated.

†Where there were significant differences in slope, the 16-day intercept was also calculated. Values connected by brackets are not significantly different.

‡The difference in slope between DEX10 and DEX70 was marginally significant ($P = 0.0513$).

§The difference in the 8-day intercept between AIB and MTX was marginally significant ($P = 0.0521$).

tively. The DEX70 accessible tissue space was largely unchanged (−5%). Therefore, DEX70 was used to calculate the vascular space. Mean intravascular plasma volume, as determined by DEX70, was 0.76 to 0.94% in BDT, BAT, and LH. ICT had a higher plasma volume than other brain samples (1.47 to 1.72%) and intravascular content was highest in the subcutaneous tumor (SQT, 2.52 to 3.29%). In both the ICT and SQT, plasma volume was slightly lower at 16 days compared with 8 days after inoculation. The corresponding mean *PS* ($\times 10^{-5}$ sec^{-1}) values in ICT for AIB, MTX, and DEX10 were 33.86, 14.14, and 7.05, respectively, at 8 days after inoculation and 72.05, 34.13, and 10.54, respectively, at 16 days after inoculation (Table 2).

The differences in accessible tissue space in ICT between the agents (differential permeability), as determined by the 8-day *y* intercept of the regression line (Table 1) was significant ($P < 0.0001$) for all agents except between MTX and DEX10 ($P = 0.2110$). Values for AIB were 4- to 5-fold greater than MTX and DEX10 and 25-fold greater than DEX70. The

Table 2. *Permeability (P) × Capillary Surface Area (S) Product at Selected Days After Inoculation of Tumor*

	PS ($sec^{-1} \times 10^{-5}$)*					
	AIB		MTX		DEX10	
Tissue	8†	16†	8	16	8	16
ICT	19.19	80.82	10.04	33.62	7.57	9.53
	48.52	63.27	18.23	34.64	6.53	11.55
	(33.86)	(72.05)	(14.14)	(34.13)	(7.05)	(10.54)
BAT	14.88	8.8	8.67	6.86	3.94	5.76
	15.03	13.98	11.56	9.71	3.26	5.64
	(14.96)	(11.39)	(10.12)	(8.29)	(3.60)	(5.70)
BDT	6.14	3.07	8.8	5.08	3.89	5.97
	6.29	8.83	3.12	6.57	3.47	4.52
	(6.22)	(5.95)	(5.96)	(5.83)	(3.68)	(5.25)
LH	8.45	4.09	8.7	5.86	3.81	5.96
	8.19	9.77	3.04	3.87	3.37	4.52
	(8.32)	(6.93)	(5.87)	(4.87)	(3.59)	(5.24)
SQT	77.62	66.1	123.52	113.18	15.16	16.12
	169.55	142.32	107.26	111.78	20.48	11.4
	(123.59)	(104.21)	(115.39)	(112.48)	(17.82)	(13.76)

*Numbers are individual animal PS values for a given agent in each tissue at 8 or 16 days after inoculation of tumor cells. Mean values are in parentheses.

†Days after inoculation.

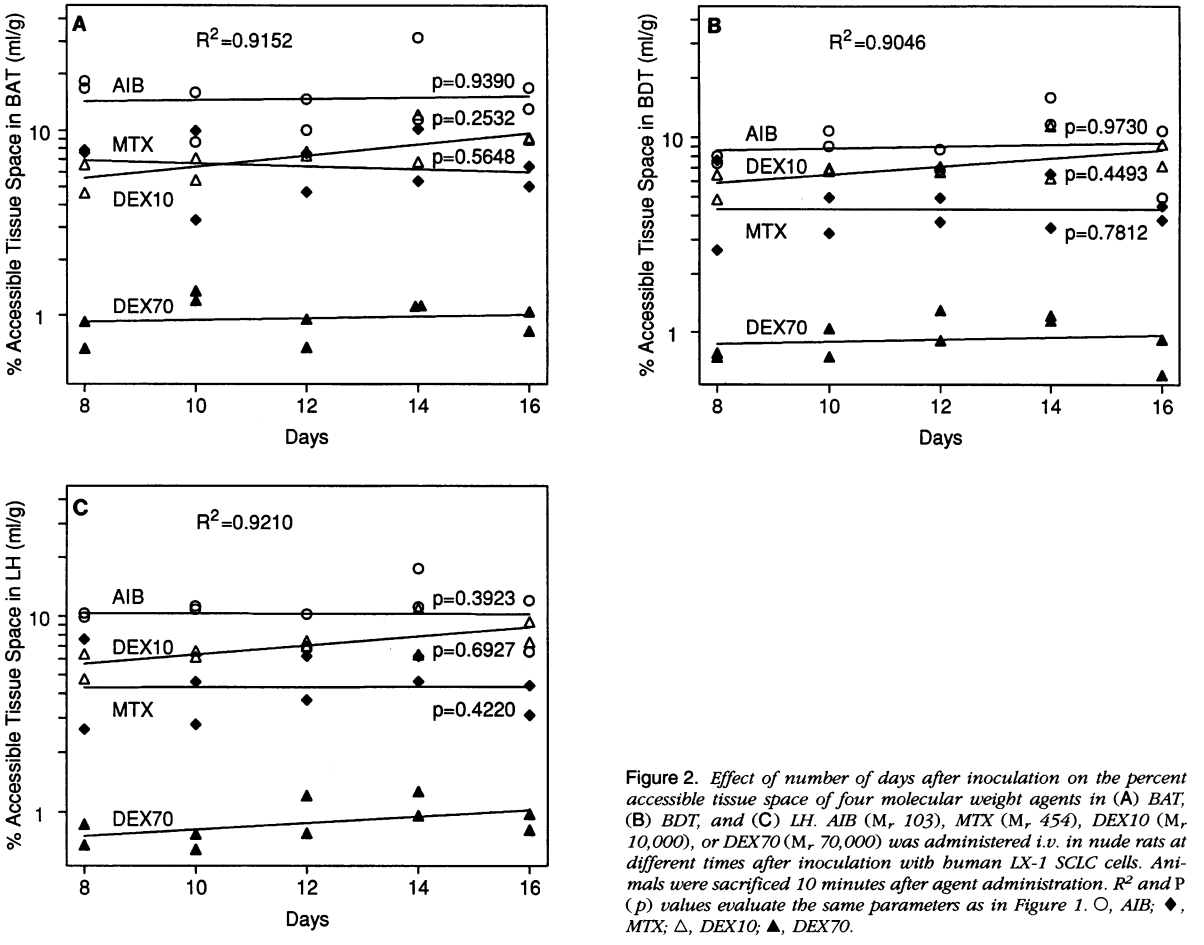

Figure 2. *Effect of number of days after inoculation on the percent accessible tissue space of four molecular weight agents in* (A) *BAT,* (B) *BDT, and* (C) *LH. AIB* (M_r *103), MTX* (M_r *454), DEX10* (M_r *10,000), or DEX70* (M_r *70,000) was administered i.v. in nude rats at different times after inoculation with human LX-1 SCLC cells. Animals were sacrificed 10 minutes after agent administration.* R^2 *and* P (*p*) *values evaluate the same parameters as in Figure 1.* ○, *AIB;* ◆, *MTX;* △, *DEX10;* ▲, *DEX70.*

differences between AIB, MTX, and DEX10 as determined by the slopes of the lines in Figure 1 and as in Table 1 were nearly constant over the 8-day experimental period. The mean *PS* values at 8 and 16 days after inoculation also demonstrated similar differences (2- to 7-fold) between AIB *versus* MTX and DEX10 (Table 2).

In the SQT, the data was model fitted (r^2 = 0.9507) and showed no significant change in the accessible tissue space with days after inoculation (Figure 1B). The mean *PS* values for AIB, MTX, and DEX10 at 8 and 16 days also showed little difference (Table 2): 123.59 and 104.21 for AIB, 115.39 and 112.48 for MTX, and 17.82 and 13.76 for DEX10. However, the differences in accessible tissue space in SQT between the agents (8-day intercept) was significant ($P < 0.001$) for all agents except between AIB and MTX for which the difference was marginal (P = 0.0521; Table 1). Values for AIB were greater than MTX, DEX10, and DEX70 by 1.7-, 5-, and 42-fold, respectively. The mean *PS* values at 8 and 16 days after inoculation show very little difference between AIB and MTX, but a 7- to 8-fold difference between AIB and MTX *versus* DEX10 (Table 2).

The effect of the number of days after inoculation on the accessible tissue space in BAT, BDT, and LH is shown in Figure 2. There was no significant change in the accessible tissue space with the number of days after inoculation. In addition, there were fewer and smaller differences between the agents (Tables 1 and 2). In all three tissues there was no significant difference in accessible tissue space between MTX and DEX10, but there was a significant difference between AIB, MTX, and DEX10 compared with DEX70. Values for AIB were greater than DEX70 by 16-, 10-, and 14-fold in BAT, BDT, and LH respectively. The *PS* values (Table 2) also showed smaller differences between AIB, MTX, and DEX10.

Both the accessible tissue space and *PS* reflect the differences in tissue permeability to each of the four agents. Accessible tissue space and *PS* were highest in the SQT and lowest in the BDT and LH. The values

in the ICT were greater than BDT and LH, but less than the SQT. The BAT was intermediate to the ICT and BDT.

The plasma disappearance half-life, expressed as a flushing rate (one/half-life), for all agents at each time point were also compared. Among each of the agents, there were no differences in the plasma flushing rate with days after inoculation ($P = 0.19$). There were also no differences between AIB, MTX, and DEX10 ($P = 0.82$). However, the plasma rate for DEX70 was significantly ($P < 0.0001$) lower, by >50%, computed with the other agents.

Survival Study

The median survival (n = 19) was 20 days (range, 14 to 26 days) with 95% of the animals developing lethal tumors (Figure 3). Survival demonstrates the natural progression of ICT growth and was the basis for the selection of days after inoculation when both permeability and volume studies were performed. Of the survival animals that were also available for histological tumor volume processing (n = 7), the mean volume was 165 ± 26 mm^3 (range, 95 to 291 mm^3). This included one animal at 16 days, five animals at 20 days, and one animal at 26 days postinoculation.

Tumor Volume Study

Animals were sacrificed at specific times between 8 and 18 days after inoculation for histological tumor volume analysis or MR imaging volume analysis to correlate with histology. Figure 4 shows representative coronal sections of the actual and computer-generated images from both histology and MR imaging at 8, 12, and 16 days after inoculation. These illustrate tumor progression, necrotic tumor center, and the tumor margins used in determining volumes. A notable portion (85%) of these tumors contained a necrotic cystic tumor component, which could be seen on both MR and histology. MR images showed the tumors to have a marked hyperintense center with surrounding areas to be hyperintense to gray matter, but not as intense as the central portion. This central area corresponded to the histological area of necrosis.

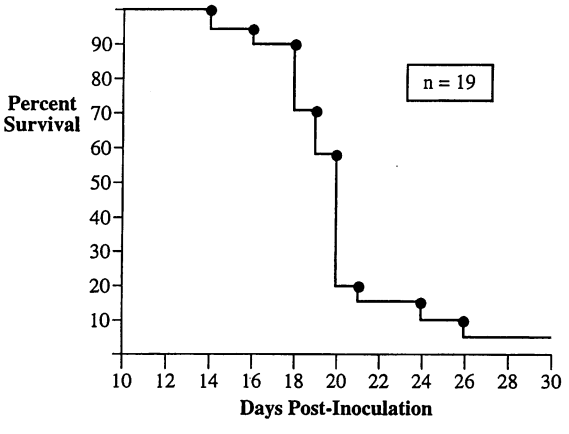

Figure 3. *Survival curve of nude rats (n = 19) stereotactically inoculated with LX-1 human SCLC cells. Median survival is 20 days (range, 14 to 26 days) with 95% of animals developing lethal ICTs.*

The calculated histology volumes at each of the time points showed some variability, but there was a consistent pattern of increasing tumor size with time. Between 8 and 16 days after inoculation, mean tumor size increased >12-fold. Figure 5 shows the correlation of all animals for which histological tumor volumes were obtained, including survival animals, with days after inoculation ($r^2 = 47.9\%$). Calculated MR imaging tumor volumes were consistently 2- to 3-fold greater than the histology volumes. On the basis of a model analysis of these animals (n = 9), MR imaging accurately correlated with histology ($r^2 = 98.5\%$) as described by: MR imaging volume = 2.2 × histology volume (residual SD = 30.2 mm^3; (Figure 6). Thus, histological volume could be predicted from MR imaging volume (MRI volume/2.2) with corresponding 95% prediction limits of ±28 mm^3.

Discussion

Tumor Permeability

Tumor cell sensitivity and drug delivery are the two major interrelated factors used to explain the lack of clinical response of brain tumors to therapy. Major factors impeding delivery are the BBB and the blood-tumor barrier[2,7,15,17,32–35] Achieving adequate drug delivery may also be limited by the risk of neurotoxicity.[28] One purpose of this study was to characterize the permeability of an ICT model as a basis for therapeutic design. To accomplish this, it was necessary to demonstrate differential permeability, defined here to be differences in a comparable quantitative measure predictive of tissue uptake between two or more agents as a result of all variables, particularly molecular weight. Thus, four biologically diverse agents with a wide range of molecular weights (100 to 70,000) were evaluated during natural tumor progression involving a wide range of ICT sizes (9 to 225 mm^3). One measure used was percent accessible tissue space, a distribution volume (ml/g) of both intravascular and extravascular components that controls for the end-point plasma concentration.[25] Another measure used (at selected time points) was the *PS*

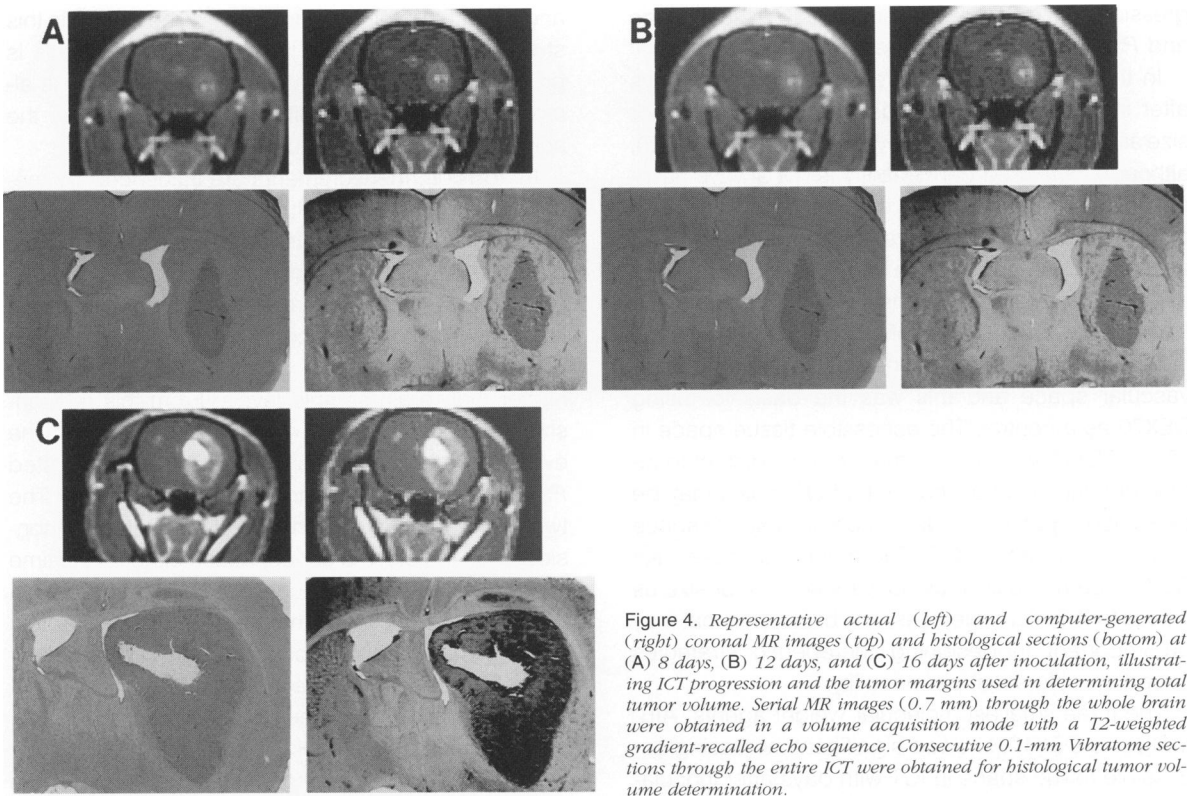

Figure 4. *Representative actual (left) and computer-generated (right) coronal MR images (top) and histological sections (bottom) at* (A) *8 days,* (B) *12 days, and* (C) *16 days after inoculation, illustrating ICT progression and the tumor margins used in determining total tumor volume. Serial MR images (0.7 mm) through the whole brain were obtained in a volume acquisition mode with a T2-weighted gradient-recalled echo sequence. Consecutive 0.1-mm Vibratome sections through the entire ICT were obtained for histological tumor volume determination.*

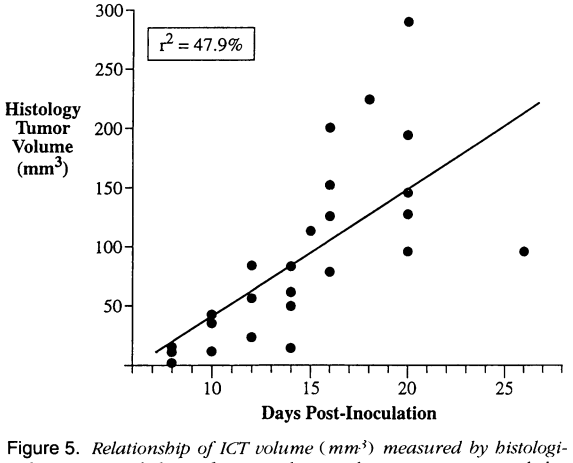

Figure 5. *Relationship of ICT volume (mm^3) measured by histological sections and days after inoculation, showing tumor growth between 8 days and the end survival in this model (n = 26).*

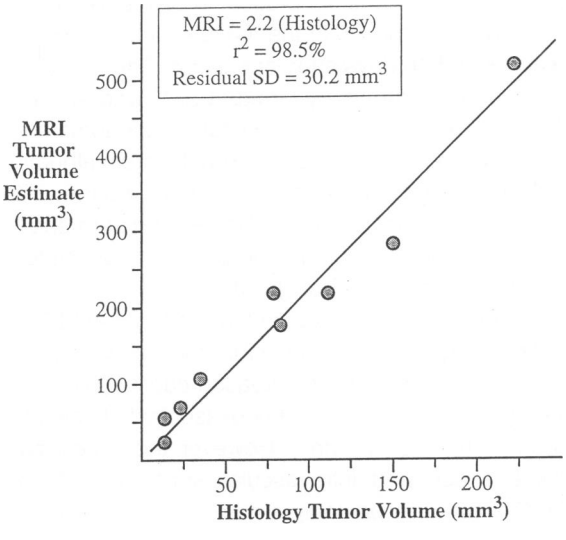

Figure 6. *Correlation of ICT volume (mm^3) determined by histological sections and MR imaging between 8 and 18 days after inoculation (n = 9).*

(permeability × capillary surface area), a time-dependent functional measure of capillary permeability from which intravascular content is subtracted.

From the analysis of this study, there were several notable results: 1), ICT accessible tissue space to three of the four agents studied significantly increased with tumor progression; 2), there was no significant change in ICT accessible tissue space to the largest molecular weight agent studied (DEX70); 3), in SQT and other brain tissues, there were no significant changes in accessible tissue space during the time studied; 4), the differential permeability between the agents was maintained over a long period of time and in the tumor samples over a large range of size; 5), intravascular volume in tumor only minimally changed, with a decreasing tendency during pro-

gression; 6), measures of accessible tissue space and *PS* yielded analogous results.

In the present study, increasing number of days after inoculation corresponded to increasing tumor size as previously reported by Zhang et al[8] (Figure 5), although increased permeability is not always associated with enlarging tumors or the development of central necrosis.[36] There was lack of change in ICT accessible tissue space to a large molecule (DEX70), even at 16 days after inoculation, which is within the lower limits of survival in this model (Figure 3). This indicates that DEX70 remained primarily in the intravascular space and this was the basis for using DEX70 as a control. The accessible tissue space in ICT to DEX70 was greater than in brain distant to tumor, but only one-half that of the SQT, which may be explained in part by the differences in vascular space in ICT, BDT, and SQT. For macromolecules like DEX70, permeability may not vary with tumor size as it does for smaller molecules, an observation that may be important in designing therapeutic strategies based on differential permeability.

The three smallest molecular weight agents, AIB, MTX, and DEX10, showed significant increasing accessible tissue space in ICT with days after inoculation, presumably from increasing disruption of the BBB. This effect was not present in BAT, BDT, LH, or SQT. Similarly, the *PS* in the ICT also increased between 8 and 16 days after inoculation. These results are similar to studies by Greig et al,[37] who studied Walker 256 experimental metastatic brain tumors in which barrier integrity, measured with serum albumin and horseradish peroxidase between 1 hour and 8 days after inoculation, showed increasing permeability and the corresponding appearance of dissociated tight junctions with tumor growth.[37]

On the basis of studies by Iannatti[38] using PET in malignant gliomas, it is possible that measured increases are the result of increased capillary surface area (S) and the increased neovascularity known to occur with tumor growth.[39] However, the accessible tissue space and intravascular space in ICT for DEX70, which is primarily a marker of intravascular volume, did not significantly change, suggesting that the capillary surface area was not a major factor in the increase in *PS* product of the smaller agents during tumor growth.

Although it was not within the scope of this study to determine the mechanisms of the observed differential permeability, several elements are suggested. For instance, three primary factors known to affect extravasation of a given agent across the BBB are lipid solubility (octanol:water partition coefficient), charge, and molecular weight (diffusivity).[29] The agents in this study are relatively lipid insoluble, and thus this is probably not a major influence, whereas there is almost a 10^2 range of diffusivity (reciprocal of the square root of the molecular weight).

In addition, measurements are influenced by metabolism, efflux, extracellular diffusion, plasma concentration, and binding to plasma and tissue components. In this study, a short 10-minute experimental period was selected to reflect primarily a unidirectional measurement (influx). Throughout the study, the plasma levels of each agent remained >10-fold higher than brain sample levels. From this relationship, unidirectional uptake can be assumed.[30] In the event some back diffusion did occur, the calculated *PS* values would be underestimated (ie, in SQT). The two different measurements used both take into consideration the plasma concentration either at the time of tissue measurement (accessible tissue space) or a time-dependent plasma integral (*PS*). It is the protein binding that probably accounts for the similar accessible tissue space measurements between MTX (which binds 50% to plasma proteins) and DEX10. This is despite a 20-fold difference in molecular weight, in effect, portraying MTX as a larger molecule subject in part to the physical factors governing macromolecules. The calculation of the *PS* includes a correction for binding to plasma proteins but also showed similar values between MTX and DEX10. The *PS* values for MTX in normal brain are in accordance with other reported studies.[31,40]

As discussed by Jain,[41] there are two significant physical factors involved in transport based on the nature of the agents in this study (small molecules *versus* macromolecules). Transport of small molecular weight agents is controlled primarily by transvascular concentration gradients or diffusion, whereas macromolecules are mostly controlled by a slower, distance-dependent transvascular pressure gradient or convection. Thus, the magnitude of differential permeability under conditions in this study may be explained in part by the convection process. In other words, the low measurements for DEX70 may be the result of the short period between agent administration and tissue sampling.

For the calculation of *PS*, DEX70 was used to determine the approximate intravascular volume because it was a large molecular weight, poorly penetrating solute in all tissues during the short experimental period. Although significant differences in vascular volume between the impermeant tracer and the test agent can occur, there was minimal correction for intravascular volume in this study. When

$C_{tissue}(T) > 3\ V_B\ C_{pls}$ (as was the case in this study), a 20% error in the measurement of intravascular space will produce less than a 10% error in the determination of *PS*.[30] The vascular volume in tumor showed a decreasing tendency with tumor growth consistent with a decreasing tumor perfusion rate and the development of necrosis.[41]

Differential permeability of brain tumors to small and large molecular weight agents has been previously described with imaging agents. By region of interest analysis, the uptake of ^{99m}Tc-glucoheptonate was much greater than ^{99m}Tc-albumin in human brain tumors.[9] In the ethylnitrosourea-induced astrocytic rat glioma model, signal intensity on MR imaging was measured after the administration of gadolinium diethylenetriamine-pentaacetic acid (Gd-DTPA), polylysine-Gd-DTPA and albumin-Gd-DTPA.[10] With increasing molecular size, a slower and less intense tumor enhancement over time was observed. The different tumor enhancement kinetics were attributed to the differential permeability of tumor capillaries for large and small molecules. In the present study, SQT also showed evidence of differential permeability, which, unlike ICT, did not change with tumor progression. This finding is consistent with other studies demonstrating abnormally high vascular permeability in SQT, allowing contrast MR imaging with albumin-Gd-DTPA.[42] Changes in permeability to albumin-Gd-DTPA in SQTs allowed distinction between nontreated tumors and those treated with tumor necrosis factor, an agent known to increase vascular permeability.

For all agents, measurements (accessible tissue space and *PS*) were highest in SQT, intermediate in ICT, lower in BAT, and lowest in BDT and LH. The ICT to normal brain ratios for these agents were <10, suggesting an abnormal but partially intact and limiting BBB. This compares with some models in which this ratio is 20 to 30 for various agents, approaching values that are thought to indicate much greater permeability than most human tumors.[7,20,32,33,43] In highly permeable animal models, efficacy studies do not account for any of the problems associated with delivery across the partially intact BBB.[33] Some studies are purposely designed to use highly permeable models, thus distinguishing cellular sensitivity and resistance from the limitation of drug accessibility.[34]

As the ICT progressed in size from 8 to 16 days after inoculation, the accessible tissue space and *PS* of AIB, MTX, and DEX10 approached, but never reached, the levels in SQT. Therapeutic predictions based on the SQT or comparisons between ICT and SQT must be guarded because of differences such as blood flow, permeability, and size[33,34,44–46] Even in the highly permeable TE-671 medulloblastoma rat model, some agents that were active in SQTs did not produce significant prolongation of survival in ICT experiments.[34]

Tumor Volumetric Measurement

Serially measuring both tumor volume and tumor necrosis in animal studies *in vivo* would permit noninvasive monitoring of response. T1-weighted contrast-enhanced MR imaging with Gd-DTPA has improved sensitivity and contrast resolution for a variety of central nervous system lesions and has proved to be a superior imaging modality.[5,47–49] Gd-DTPA is distributed extracellularly and is primarily a marker of an abnormal BBB.[10,50–52]

Only a few studies in animal brain tumor models have used MR imaging.[18,19,51,53,54] In the RG-C6 rat glioma model in which a single slice two-dimensional measurement was obtained, tumor size on contrast-enhanced MR imaging tended to be larger than the histological section.[52] By visual inspection, MR imaging correlated well with gross pathological findings in a canine gliosarcoma model.[53] In a subsequent study in this model, serial 3-mm images were obtained to calculate three-dimensional volumes with different imaging protocols, but no comparison was made with histological sections.[18] In rats with 9L glioma tumors, volumes were calculated from serial 2- to 3-mm images on a 4.7 Tesla high magnetic field strength unit. Accuracy of the calculation in that report depended on spherical tumor symmetry but did show good visual correlation with histology.[19]

In this study, we applied similar consecutive sectioning to both MR images and histological sections. Three-dimensional tumor volumes were calculated in an identical manner for both histology and imaging data with software designed for this purpose. Tumor progression was measured from serial histological tumor sections between 8 days after inoculation and death (Figure 5). There was progressive tumor enlargement over time with a wide range of measured volumes, particularly with older tumors. This same pattern of variability was demonstrated in the 9L glioma model and was thought to reflect animal-to-animal variability.[19] In the present model, studies are continuing to evaluate volume variability.

Tumor volumes calculated from serial 0.7-mm images on contrast-enhanced MR imaging invariably and predictably overestimated tumor size compared with the histological values (Figure 6). The correlation (r^2 = 98.5%) permitted a predicted histology volume

from MR imaging of 0.4545 × MR imaging volume. It was assumed that the histological volumes provided the most accurate measurements, although there may be as much as 10% shrinkage of tissue during formalin processing. The reason for the volume differences between MR imaging and histology is unclear. The possibility of calibration or mathematical error was thoroughly investigated and no such errors were found. One potential explanation is a rapid diffusion of Gd-DTPA from tumor to surrounding tumor-free tissue.[54] In a preliminary study in this model, we did not observe any changes attributable to diffusion between immediate postcontrast scans and 30 minutes after contrast, but more studies are needed to confirm this result. Dissociation of the Gd chelate is unlikely to be a factor inasmuch as acid dissociation is associated with longer residence intervals (>1 day).[55] As previously described, slicing errors and partial volume effects can result in over- or underestimation, but these would affect small volume tumors more and would decrease as slice thickness decreases and resolution increases.[18] If slicing error had been present, it was presumably small and consistent over a large range of tumor volumes. Thus, no adequate explanation exists for the 2.2-fold difference in volume measured by MR imaging and histology. Nonetheless, volumes obtained from MR imaging remain a consistent measure of histological volumes and are therefore useful as a predictor.

In conclusion, this study characterizes a model that demonstrates differential permeability of ICTs to small and large molecular weight agents for future investigation of novel therapeutic approaches. The baseline information obtained in the untreated animals will assist in the optimal design of future experiments. The ability to measure tumor volumes and necrosis with serial *in vivo* MR imaging and from histological sections will likely provide valuable information regarding therapeutic efficacy.

Acknowledgments

We express our appreciation to David Wilson for data evaluation and graphics.

Appendix

In using a multiple regression model to estimate rates of uptake in tissue as a function of time we denote the response variable by y whereas the independent variable, time, is denoted by x_1. We also introduce indicator variables x_2, x_3, and x_4 where $x_2 = 1$ if the agent is AIB and 0 otherwise, $x_3 = 1$ if the treatment is MTX and 0 otherwise, $x_4 = 1$ if the treatment is DEX10 and 0 otherwise. In this context we have arbitrarily chosen DEX70 as a reference treatment. To estimate differences in level at 8 days (intercept) and differences in rates of change with respect to time for each treatment, we fit a multiple regression model including interaction terms.

We are assuming that a given observation may be expressed as $E(Y) = \beta_0 + \beta_1 x_1 + \beta_2 x_2 + \beta_3 x_3 + \beta_4 x_4 + \beta_5 x_1 x_2 + \beta_6 x_1 x_3 + \beta_7 x_1 x_4$, where $E(y)$ represents the average response, β represents parameters to be estimated by least squares and the x is defined as above. The fitting and interpretation of this model follows the standard treatment when using indicator variables.[26,27] We summarize briefly here the specifics of this model.

Model Interpretation

To understand the meaning of the parameters of this model we consider first the case of the treatment of 10 animals with DEX70. For this treatment, $x_2 = 0$, $x_3 = 0$, and $x_4 = 0$, and we have $E(y) = \beta_0 + \beta_1 x_1 + \beta_2(0) + \beta_3(0) + \beta_4(0) + \beta_5 x_1(0) + \beta_6 x_i(0) + \beta_7 x_1(0)$, which reduces to $E(y) = \beta_0 + \beta_1 x_1$.

Thus, the response function for DEX70 is a straight line with intercept β_0 and slope β_1. When the treatment is DEX10, $x_2 = 0$, $x_3 = 0$, and $x_4 = 1$ and the model becomes $E(Y) = \beta_0 + \beta_1 x_1 + \beta_2(0) + \beta_3(0) + \beta_4(1) + \beta_5 x_1(0) + \beta_6 x_1(0) + \beta_7 x_1(1)$, which reduces to $E(y) = (\beta_0 + \beta_4) + (\beta_1 + \beta_7)x_1$.

The response function for DEX10 is a straight line with intercept $\beta_0 + \beta_4$ and slope $\beta_1 + \beta_7$. Similarly, for MTX, $E(y) = (\beta_0 + \beta_3) + (\beta_1 + \beta_6)x_1$, and for AIB, $E(y) = (\beta_0 + \beta_2) + (\beta_1 + \beta_5)x_1$.

The meaning of the parameters in the response function is now clear. Parameters β_2 and β_5 represent differences in the intercepts and slopes, respectively, for AIB as compared with DEX70. Similarly, β_3 and β_6 represent differences in slope and intercept for MTX whereas β_4 and β_7 represent corresponding differences for DEX10 as compared with DEX70. An advantage of using a single unified model, incorporating all agents, to estimate rates of change over time rather than fit individual regressions for each agent is that inferences regarding regression parameters can be made more precisely by working with one regression model containing indicator variables, as more degrees of freedom will then be associated with the mean of the squared errors. That is, with 10 animals per group, the degrees of freedom associated with

estimating the error is 8 for each individual regression whereas a single model results in 32 degrees of freedom.

Although we have referenced all comparisons in the fitted model to DEX70, comparisons between other agents are easily obtained. For example, to compare MTX with AIB, differences in intercepts are given by $\beta_3 - \beta_2$, and differences in slopes are found from $\beta_6 - \beta_5$. Letting b_i denote the regression estimate of β_1, i = 1, . . . 7, the regression estimates of these differences are found from $b_3 - b_2$ and $b_6 - b_5$, respectively. The estimated variances in these estimators is var $(b_i - b_j)$ = var (b_i) + var (b_j) – 2cov (b_i, b_j) where var denotes variance and cov denotes covariance. These variances and covariances are easily obtained from the estimated variance-covariance matrix of the regression coefficients.

Intercepts traditionally taken at the origin are often not biologically relevant. Intercepts taken at biologically relevant points are easily obtained by a translation of the data. For example, 8-day intercepts are found by translation of the time axis by coding time as calendar time – 8. The fitted intercepts will now represent the intercept at 8 days.

References

1. Groothuis DR, Lapin GD, Vriesendorp FJ, Mikhael MA, Patlak CS: A method to quantitatively measure transcapillary transport of iodinated compounds in canine brain tumors with computed tomography. J Cereb Blood Flow Metab 1991, 11:939–948
2. Yamada K, Ushio Y, Hayakawa T, Kato A, Yamada N, Mogami H: Quantitative autoradiographic measurements of blood-brain barrier permeability in the rat glioma model. J Neurosurg 1982, 57:394–398
3. Nir I, Levanon D, Iosilevsky G: Permeability of blood vessels in experimental gliomas: uptake of ^{99m}Tc-glucoheptonate and alteration in blood-brain barrier as determined by cytochemistry and electron microscopy. Neurosurgery 1989, 25:523–532
4. Burger PC, Heinz ER, Shibata T, Kleihues P: Topographic anatomy and CT correlations in the untreated glioblastoma multiforme. J Neurosurg 1988, 68:698–704
5. Sze G, Milano E, Johnson C, Heier L: Detection of brain metastases: comparison of contrast-enhanced MR with unenhanced MR and enhanced CT. AJNR 1990, 11:785–791
6. Kelly PJ, Daumas-Duport C, Kispert DB, Kall BA, Scheithauer BW, Illig JJ: Imaging-based stereotaxic serial biopsies in untreated intracranial glial neoplasms. J Neurosurg 1987, 66:865–874
7. Groothuis DR, Vriesendorp FJ, Kupfer B, Warnke PC, Lapin GD, Kuruvilla A, Vick NA, Mikhael MA, Patlack CF: Quantitative measurements of capillary transport in human brain tumors by computed tomography. Ann Neurol 1991, 30:581–588
8. Zhang R, Price JE, Fijimaki T, Bucana CD, Fidler IJ: Differential permeability of the blood-brain barrier in experimental brain metastases produced by human neoplasms implanted into nude mice. Am J Pathol 1992, 141:1115–1124
9. Neuwelt EA, Specht HD, Hill SA: Permeability of human brain tumor to ^{99m}Tc-glucoheptonate and ^{99m}Tc-albumin implications for monoclonal antibody therapy. J Neurosurg 1986, 65:194–198
10. Schmiedl UP, Kenney J, Maravilla KR: Kinetics of pathologic blood-brain barrier permeability in an astrocytic glioma using contrast-enhanced MR. AJNR 1992, 13:5–14
11. Kato Y, Paterson A, Langone JJ: Monoclonal antibodies to chemotherapeutic agent methotrexate: production, properties, and comparison with polyclonal antibodies. J Immune Methods 1984, 67:321–326
12. Curd J: The isolation of digoxin-specific antibody and its use in reversing the effects of digoxin. Proc Natl Acad Sci USA 1971, 68:2401–2406
13. Senter PD, Saulnier MG, Schreiber GJ, Hirschberg DL, Brown JP, Hellström I, Hellström KE: Antitumor effects of antibody-alkaline phosphatase conjugates in combination with etoposide phosphate. Proc Natl Acad Sci USA 1988, 85:4842–4846
14. Senter PD, Schreiber GJ, Hirschberg DL, Ashe SA, Hellström KE, Hellström I: Enhancement of the *in vitro* and *in vivo* antitumor activities of phosphorylated mitomycin C and etoposide derivatives by monoclonal antibody-alkaline phosphatase conjugates. Cancer Res 1989, 49:5789–5792
15. Lee Y, Bullard DE, Humphrey PA, Colapinto EV, Friedman HS, Zalutsky MR, Coleman RE, Bigner DD: Treatment of intracranial human glioma xenografts with ^{131}I-labeled antitenascin monoclonal antibody 81C6. Cancer Res 1988, 48:2904–2910
16. Nazzaro JM, Pagel M, Rosenbaum L, Neuwelt EA: A new model of systemic drug rescue based on permeability characteristics of the blood-brain barrier in intracerebral abscess-bearing rats. J Neurosurg 1991, 74:467–474
17. Robinson PJ, Rapoport SI: Model for drug uptake by brain tumors: effects of osmotic treatment and diffusion in brain. J Cereb Blood Flow Metab 1990, 10:153–161
18. Galloway RL, Maciunas RJ, Failinger AL, Whelan HT. Volumetric measurement of canine gliomas using MRI. Magnetic Resonance Imaging 1990, 8:161–165
19. Rajan SS, Rosa L, Francisco J, Muraki A, Carvlin M, Tuturea E. MRI characterization of 9L-glioma in rat brain at 4.7 tesla. Magnetic Resonance Imaging 1990, 8:185–190
20. Lee Y-S, Bullard DE, Zalutsky MR, Coleman RE, Wikstrand CJ, Friedman HS, Colapinto EV, Bigner DD:

Therapeutic efficacy of antiglioma mesenchymal extracellular matrix ^{131}I-radiolabeled murine monoclonal antibody in a human glioma xenograft model. Cancer Res 1988, 48:449–566

21. Wheeler KT: Review of factors influencing the response of experimental brain tumors to therapy. Cancer Treat Rep 1981, 65:74–81
22. Kallman RF, Brown JM, Denekamp J, Hill RP, Kummermehr J, Trott K-R: The use of rodent tumors in experimental cancer therapy: conclusions and recommendations from an internal workshop. Cancer Res 1985, 45:6541–6545
23. Neuwelt EA, Barnett PA, Ramsey FL, Hellström I, Hellström KE, McCormick CI: Dexamethasone decreases the delivery of tumor-specific monoclonal antibody to both intracerebral and subcutaneous tumor xenografts. Neurosurgery 1993, 33:478–484
24. Neuwelt EA, Frenkel E, D'Agostino AN, Carney DN, Minna JD, Barnett PA, McCormick CI: Growth of human lung tumor in the brain of the nude rat as a model to evaluate antitumor agent delivery across the blood-brain barrier. Cancer Res 1985, 45:2827–2833
25. Reed DJ, Woodbury DM: Kinetics of movement of iodine, sucrose, insulin and radioiodinated serum albumin in the CNS and CSF of the rat. J Physiol 1963, 169:816–850
26. Neter J, Wasserman W, Kutner MH: Applied Linear Regression Models. Chicago, Richard D. Irwin, 1983
27. Kleinbaum DG, Kupper LL, Muller KE: Applied Regression Analysis and Other Multivariable Methods, ed 2. PWS-Kent, a division of Wadsworth, Belmont, CA 1988
28. Neuwelt EA, Barnett PA: Blood-brain barrier disruption in the treatment of brain tumors: animal studies. Neuwelt EA ed. Implications of the Blood-Brain Barrier and Its Manipulation: Clinical Implications, vol 2. Edited by EA Neuwelt. New York, Plenum Press, 1989, pp 107–194
29. Fenstermacher JD: Current models of blood-brain transfer. Trends Neurosci 1985, October:449–453
30. Smith QR: Quantitation of blood-brain barrier permeability. In Neuwelt EA ed.: Implications of the Blood-Brain Barrier and Its Manipulation: Basic Science Aspects, vol 1. Edited by EA Neuwelt. New York, Plenum Press, 1989, pp 85–113
31. Neuwelt EA, Barnett PA, Frenkel EP: Chemotherapeutic agent permeability to normal brain and delivery to avian sarcoma virus-induced brain tumors in the rodent: observations on problems of drug delivery. Neurosurgery 1984, 14:154–160
32. Vriesendorp FJ, Peagram C, Bigner DD, Groothuis DR: Concurrent measurements of blood flow and transcapillary transport in xenotransplanted human gliomas in immunosuppressed rats. Natl Cancer Inst 1987, 79: 123–130
33. Warnke PC, Friedman HS, Bigner DD, Groothuis DR: Simultaneous measurements of blood flow and blood-to-tissue transport in xenotransplanted medulloblastomas. Cancer Res 1987, 47:1687–1690
34. Friedman HS, Schold SC, Bigner DD: Chemotherapy of subcutaneous and intracranial human medulloblastoma xenografts in athymic nude mice. Cancer Res 1986, 46:224–228
35. Groothuis DR, Fischer JM, Vick NA, Bigner DD: Comparative permeability of different glioma models to horseradish peroxidase. Curr Cancer Rep 1981, 65: 13–18
36. Molnar P, Blasberg RG, Groothuis D, Bigner D, Fenstermacher JD: Regional blood-to-tissue transport in avian sarcoma virus (ASV)-induced brain tumors. Neurology 1983, 33:702–711
37. Greig N, Jones H, Cavanagh J: Blood-brain barrier integrity and host responses in experimental metastatic brain tumors. Clin Exp Metastasis 1983, 1:229–246
38. Iannotti F: Functional imaging of blood-brain barrier permeability by single photon emission computerized tomography in positron emission tomography. Advances and Technical Standards in Neurosurgery. Edited by L Symon. Berlin, Springer Verlag 1992, pp 103–118
39. Yamada K, Hayakawa T, Ushio Y, Arita N, Kato A, Mogami H: Regional blood flow and capillary permeability in the ethylnitrosourea-induced rat glioma. J Neurosurg 1981, 55:922–928
40. Ohata M, Fredericks WR, Neuwelt EA, Sundaram U, Rapoport SI: [^{3}H]Methotrexate loss from the rat brain following enhanced uptake by osmotic opening of the blood-brain barrier. Cancer Res 1985, 45:1092–1096
41. Jain RK: Haemodynamic and transport barriers to the treatment of solid tumors. Int J Radiat Biol 1991, 60(1/2):85–100
42. Aicher KP, Dupon JW, White DL, Aukerman SL, Moseley ME, Juster R, Rosenau W, Winkelhake JL, Brasch RC: Contrast-enhanced magnetic resonance imaging of tumor-bearing mice treated with human recombinant tumor necrosis factor α. Cancer Res 1990, 50: 7376–7381
43. Blasberg RG, Groothuis D, Molnar P: A review of hyperosmotic blood-brain barrier disruption in seven experimental brain tumor models. Johanson Pathophysiology of the Blood-brain Barrier. Edited by BB Johanson, CH Owman, H Widner. Amsterdam, Elsevier, 1990, p. 197
44. Hagan PL, Halpern SE, Dillman RO, Shawler DL, Johnson DE, Chen A, Krishnan L, Frincke J, Bartholomew RM, David GS, Carlo D: Tumor size: effect on monoclonal antibody uptake in tumor models. J Nucl Med 1986, 27:422–427
45. Schold SC, Rawlings CE, Bigner SH, Bigner DD: Intracerebral growth of a human glioma tumor line in athymic mice and treatment with procarbazine, 1,3-*Bis*(2-chloroethyl)-1-nitrosourea, aziridinylbenzoquinone, and *cis*-platinum. Neurosurgery 1983, 12:672–677

46. Genka S, Deutsch J, Stahle PL, Shetty UH, John V, Robinson C, Rapoport SI, Greig NH: Brain and plasma pharmacokinetics and anticancer activities of cyclophosphamide and phosphoramide mustard in the rat. Cancer Chemother Pharmacol 1990, 27:1–7
47. Davis PC, Hudgins PA, Peterman SB, Hoffman JC: Diagnosis of cerebral metastases: double-dose delayed CT vs. contrast-enhanced MR imaging. AJNR 1991, 12:293–300
48. Russell EJ, Geremia GK, Johnson CE, Huckman MS, Ramsey RG, Washburn-Bleck J, Turner DA, Norusis M: Multiple cerebral metastases: detectability with Gd-DTPA-enhanced MR imaging. Radiology 1987, 165: 609–617
49. Healy ME, Hesselink JR, Press GA, Middleton MS: Increased detection of intracranial metastases with intravenous Gd-DTPA. Radiology 1987, 165:619–624
50. Yoshida K, Furuse M, Kaneoke Y, Saso K, Inao S, Motegi Y, Ichihara K, Izawa A: Assessment of T1 time course changes and tissue-blood ratios after Gd-DTPA administration in brain tumors. Magnetic Resonance Imaging 1989, 7:9–15
51. Runge VM, Jacobson S, Wood ML, Kaufman D, Adelman LS: MR imaging of rat brain glioma: Gd-DTPA versus Gd-DOTA. Radiology 1988, 166:835–838
52. Baba T, Moriguchi M, Natori Y, Katsuki C, Inoue T, Fukui M: Magnetic resonance imaging of experimental rat brain tumors: histopathological evaluation. Surg Neurol 1990, 34:378–382
53. Whelan HT, Clanton JA, Moore PM, Tolner DJ, Kessler RM, Whetsell WO. Magnetic resonance brain tumor imaging in canine glioma. Neurology 1987, 37:1235–1239
54. Bockhorst K, Hoehn-Berlage M, Kocher M, Hossmann K-A: MRI contrast enhancement by MnTPPS of experimental brain tumours in rats. Acta Neurochir 1990, 51: 134–136
55. Wedeking P, Kumar K, Tweedle MF: Dissociation of gadolinium chelates in mice: relationship to chemical characteristics. Magnetic Resonance Imaging 1992, 10:641–648